Relativistic *N*th order muffin-tin orbital theory

L. Tsetseris* and O. Jepsen
Max-Planck-Institut für Festkörperforschung, Heisenbergstrasse 1, D-70569 Stuttgart, Germany
(Received 13 September 2004; revised manuscript received 15 December 2004; published 26 May 2005)

The muffin-tin orbital (MTO) method has been generalized to arbitrary (*N*th) order in the energy expansion of the partial waves and discrete energy meshes. This so-called NMTO method can provide energies and wave functions in a broad energy window, with controlled errors and without increasing the size of the basis set. Here we present the fully relativistic version of the NMTO method. Several tests of the applicability of the method are provided for both nonmagnetic and magnetic solids.

DOI: 10.1103/PhysRevB.71.195115 PACS number(s): 71.15.Ap

I. INTRODUCTION

The muffin-tin-orbital (MTO) method[1] has been one of the most popular *ab initio* methods for calculating the electronic structure of solids. An important feature of the method is that it uses a *minimal* basis set of orbitals. These are constructed from the exact solutions of the muffin-tin (MT) approximation to the one-electron potential. A *linear* muffin-tin orbital (LMTO) is a decaying free-particle solution found in the interstitial region between the MT spheres and continuing smoothly inside the spheres. Inside a sphere, it is a linear combination of a solution of Schrödinger's equation for the spherical potential at a chosen energy ϵ_ν and its *first* energy derivative (Taylor approximation).

A commonly used approach that enhances the efficiency of the method is the so-called atomic-sphere approximation (ASA).[2,3] This approximation amounts to two conditions that the variational basis is set to satisfy: (i) all interstitial solutions have the same kinetic energy, usually zero, and (ii) only the central part of the potential inside-space-filling spheres is used. There have been various successful attempts to improve the calculations beyond ASA. These attempts range from including the so-called combined correction[2,3] to solving for a nonspherical representation of the potential in the spheres. The latter approach leads to the full potential (FP) LMTO methods.[4,5] (For an overview of the developments around LMTO see Ref. 6 and references therein.) FPLMTO can be close to or away from the golden ratio of accuracy over efficiency, and this depends, of course, on the problem of interest and the available computational power.

A few years ago the third generation LMTO (Refs. 7–9) (in the present paper denoted as LMTO3) method was introduced. Within LMTO3, tails and heads have the same ϵ_ν energies. Moreover, the LMTO3 screening transformation is given by a certain boundary condition that aims to derive maximally localized orbitals in a physically transparent way. The ideas behind LMTO3 have been subsequently enriched and transformed to the new *N*th order MTO (NMTO) method.[6,10] NMTO is based on a suitable interpolation scheme that goes beyond the Taylor approximation of the LMTO and can provide basis orbitals of arbitrary (*N*th) order. It can describe the band energies with high accuracy in an energy window, the position and width of which can be chosen at will. Using NMTO one can obtain low-lying semicore and high unoccupied band states without increasing the size of the basis set. Moreover, the method can provide, through the downfolding procedure, Wannier functions for the description of any isolated set of bands.[11]

In the present paper we discuss the fully relativistic version of the NMTO (RNMTO) method. RNMTO follows in the steps of previous relativistic LMTO approaches,[12–17] but it is based completely on the new formalism and has the corresponding advantages. After presenting the basic formalism, we demonstrate its applicability for nonmagnetic and magnetic solids alike. Here we restrict ourselves to the introduction of the new method. Further applications, concerning, for example, calculations of optical spectra, will be presented elsewhere.

II. METHOD

We start by introducing two different sets of spheres. The first set is called the Wigner-Seitz (WS) or potential spheres, with $s_{\mathbf{R}}$ being the radius of the WS sphere that surrounds a nucleus centered at position $\mathbf{R}$. These are the standard WS spheres used in any MT construction. The head of an RNMTO will include the solution to the MT potential from the center up to $s_{\mathbf{R}}$. We term this solution a *partial wave*. The second set of spheres is the so-called screening or charge spheres, and they are used to define the boundary conditions that the interstitial solutions [termed *screened spherical waves* (SSW)] obey. As we will see below, because of the nature of the boundary conditions, screening spheres lie in general within the *s* spheres. In the region between the two sets of spheres, we solve the free wave equation to find the so-called *back extrapolated wave*.

For a central field, solutions of the nonrelativistic Schrödinger and the scalar-relativistic Pauli equations are classified by the combined quantum number $L=(l,m)$, where l and m are the orbital angular momentum and its z projection, respectively. In the absence of a magnetic field, the solutions of Dirac's equation for a spherical potential are distinguished with the index Λ, which is a combined quantum number of the total angular momentum j and its z projection μ. More details about the Dirac equation and the classification of its solutions can be found in Appendix A

and, in more detail, in Refs. 18 and 19. In the following, any object that carries an L (Λ) subscript refers to a nonrelativistic (relativistic) quantity. Relativistic wave functions are bispinors with upper and lower components.

A. Screened spherical waves

The interstitial solutions are solutions of the Dirac equation for the constant potential V_{mtz}. Their upper and lower components are Neumann or Bessel functions, which are denoted by n_{RL} and j_{RL}, respectively (with the bispinors denoted by $N_{R\Lambda}$ and $J_{R\Lambda}$). From these long-range *canonical* solutions, we construct the screened relativistic Neumann ($N^{\alpha}_{R\Lambda}$) and Bessel ($J^{\alpha}_{R\Lambda}$) functions, that satisfy the following boundary conditions on the screening spheres with radius $a_{R'\Lambda'}$:

$$N^{\alpha}_{1,R\Lambda}(a_{R\Lambda}) = 1,$$

$$J^{\alpha}_{1,R\Lambda}(a_{R'\Lambda'}) = 0, \quad \forall\, a_{R'\Lambda'}, \tag{1}$$

where the subscript 1 is used to denote the upper component. In words, a screened solution is required to have pure Λ character on its own sphere and to vanish on all other spheres. These conditions are incompatible with a set of overlapping screening spheres, and they are satisfied through the transformation,

$$N^{\alpha}_{R\Lambda} = t_1 N_{R\Lambda} + t_2 J_{R\Lambda},$$

$$J^{\alpha}_{R\Lambda} = t_3 N_{R\Lambda} + t_4 J_{R\Lambda}. \tag{2}$$

If we also impose the conditions $N'^{\alpha}_{1,R\Lambda}(a_{R\Lambda})=0$ and $J'^{\alpha}_{2,R\Lambda}(a_{R\Lambda})=1$ for the slopes of the upper components, we find

$$\begin{bmatrix} t_1 & t_2 \\ t_3 & t_4 \end{bmatrix} = \frac{1}{n_l j_{l\pm1} - j_l n_{l\pm1}} \begin{bmatrix} j_{l\pm1} & -n_{l\pm1} \\ -\dfrac{p}{\gamma} j_l & \dfrac{p}{\gamma} n_l \end{bmatrix}. \tag{3}$$

In the above, $\gamma = 1 + E - V_{mtz}/c^2$, $p = \sqrt{(E - V_{mtz})\gamma}$, and $\pm$ is used to distinguish the cases of $\kappa = -l-1$, l, respectively.

The canonical, relativistic Neumann functions at one site can be expanded at another site in a spin-spherical harmonic basis. In a complete analogy to the nonrelativistic case, it can be shown that the radial-part dependence at any other site is given by a linear combination of Bessel functions, and the coefficients determine the so-called canonical, relativistic structure constants $S^0_{R'\Lambda',R\Lambda}$. Formally,

$$N_{R\Lambda} = -\sum_{\Lambda'} J_{R'\Lambda'} S^0_{R'\Lambda',R\Lambda}. \tag{4}$$

The $S^0_{R'\Lambda',R\Lambda}$ matrix can be obtained from the nonrelativistic one ($S^0_{R'L',RL}$) by a unitary transformation from the $L=(l,m)$ basis to the $\Lambda=(\kappa,\mu)$ one,

$$S^0_{R'\Lambda',R\Lambda} = \sum_{\sigma=\pm 1/2} c(l'j';\mu'-\sigma,\sigma) S^0_{R'L',RL} c(lj;\mu-\sigma,\sigma), \tag{5}$$

where $c(lj;m,\sigma)$ are the appropriate Clebsch-Gordan coefficients.

In analogy to the canonical case, the relativistic (bispinor) SSW $\Psi_{R\Lambda}$ is given by an expansion of the form,

$$\Psi_{R\Lambda} = N^{\alpha}_{R\Lambda}\delta_{R',R} - \sum_{\Lambda'} J^{\alpha}_{R'\Lambda'} S^{\alpha}_{R'\Lambda',R\Lambda}. \tag{6}$$

The screened relativistic structure constants S^{α} are then determined through the t_i's and the matrix S^0,

$$S^{\alpha} = \frac{t_1}{t_3} + \frac{1}{t_3}\left(-\frac{t_4}{t_3} - S^0\right)^{-1} \frac{1}{t_3}[t_1 t_4 - t_2 t_3]. \tag{7}$$

Finally, by using Green's second theorem, and considering the fact that the value of the lower component in all screening spheres is given by $S^{\alpha}_{R'\Lambda',R\Lambda}$, we arrive at an important relation for the overlap integral,

$$\langle \Psi_{R\Lambda}(E_1) | \Psi_{R'\Lambda'}(E_2) \rangle = \frac{S^{\alpha}_{R\Lambda,R'\Lambda'}(E_1) - S^{\alpha}_{R'\Lambda',R\Lambda}(E_2)}{E_1 - E_2}. \tag{8}$$

B. Partial- and back-extrapolated waves

Inside the WS spheres, one has to integrate the Dirac equation *outward* from the nucleus to $s_{\mathbf{R}}$ to find the partial waves $\varphi_{R\Lambda}(E,\mathbf{r})$. In the conventional LMTO, one would then augment the tails right at the WS sphere with a combination of φ and its energy derivative $\dot{\varphi}$. In the third generation MTO, however, the situation is different. Since we have defined the boundary or screening condition for the SSW's on a different set of spheres (the set of *a* spheres), the augmentation will also take place on that set. To make this possible, we integrate the Dirac equation for a flat potential V_{mtz} *inward* from the $s_{\mathbf{R}}$ to the $a_{\mathbf{R}\Lambda}$ screening radius to obtain the so-called *back-extrapolated wave* $\varphi^0_{R\Lambda}(E,\mathbf{r})$. As we said before, because of the nature of the boundary condition on SSW, *a* spheres in general lie within potential spheres. For φ^0 we require that it matches φ at s_R both for the upper and the lower components. The wave functions φ^0 and φ are then normalized with the condition that

$$\varphi^0_{1,R\Lambda}(E, a_{R\Lambda}) = 1, \tag{9}$$

where 1 as subscript denotes again the upper component.

We define at this point the *relativistic kinked partial wave* (RKPW),

$$\Phi_{R\Lambda} = \varphi_{R\Lambda} - \varphi^0_{R\Lambda} + \Psi_{R\Lambda}. \tag{10}$$

By construction, the upper component of $\Phi_{R\Lambda}$ is continuous everywhere, but its slope, or, equivalently, the value of its lower component, has discontinuities at each $a_{R\Lambda}$ sphere. The discontinuity of the $R'\Lambda'$ projection of $\Phi_{R\Lambda}$ is given by the *kink matrix*,

$$K_{R'\Lambda',R\Lambda}(E) \equiv a_{R\Lambda} D^{\alpha}_{R\Lambda}(E)\delta_{R\Lambda,R'\Lambda'} - a_{R'\Lambda'} S^{\alpha}_{R'\Lambda',R\Lambda}(E), \tag{11}$$

where

$$D^{\alpha}_{R\Lambda}(E) \equiv \frac{1}{\varphi^{0}_{1,R\Lambda}(E,a_{R\Lambda})} \left.\frac{\partial \varphi^{0}_{1,R\Lambda}(E,r)}{\partial r}\right|_{a_{R'\Lambda'}}, \tag{12}$$

is the logarithmic derivative and $S^{\alpha}_{R'\Lambda',R\Lambda}(E)$ gives the change in the slope (kink) of the upper component of the $R'\Lambda'$ projection of a SSW $\Psi_{R\Lambda}(E,\mathbf{r})$ as it enters the $a_{R'\Lambda'}$ sphere. Solving of the Schrödinger problem for a solid amounts to forming the right linear combination of RKPW's,

$$\psi = \sum_{R\Lambda} \Phi_{R\Lambda} c_{R\Lambda}, \tag{13}$$

so that there is a cancellation of all kinks [Korringa-Kohn-Rostoker (KKR) secular equation],

$$\sum_{R\Lambda} K_{R'\Lambda',R\Lambda}(E) c_{R\Lambda} = 0. \tag{14}$$

In the relativistic case, we can choose to apply the condition that either the kinks of the upper or the *discontinuities* of the lower components vanish on the $a_{R\Lambda}$ spheres. The two approaches, must of course, give the same results. Indeed, it is easy to show (details are given in Appendix A), that the secular equation eliminates both the kinks of the upper and the discontinuities of the lower components. Let us also mention here that the choice of boundary conditions for the screened spherical waves is largely arbitrary. The key point is that for each set of conditions, a secular equation similar to Eq. (14) can be constructed, so that it eliminates both kinks and discontinuities and provides solutions to the fully relativistic (Dirac) problem.

Using the fact that the kinks of the RKPW's are related to the K matrix, it is straightforward to find the result of the Hamiltonian operator acting on such a function,

$$(\hat{H} - E)\Phi_{R\Lambda}(E,\mathbf{r}) = \sum_{R'\Lambda'} \delta(r_{R'} - a_{R'\Lambda'}) \frac{\Omega_{R'\Lambda'}(\hat{\mathbf{r}}_{R'})}{a_{R'\Lambda'} a_{R'\Lambda'}} K_{R'\Lambda',R\Lambda}, \tag{15}$$

and from this we obtain for the Hamiltonian matrix,

$$\langle \Phi | \hat{H} | \Phi \rangle = E \langle \Phi | \Phi \rangle + K. \tag{16}$$

Thus, we arrive at the important relation that the inverse of the Kink matrix gives the Green matrix (resolvent) of the problem with a minus sign.

Likewise, by using Green's second theorem, one can deduce the second important relation that provides the overlap matrix,

$$\langle \Phi(E_1) | \Phi(E_2) \rangle = \frac{K_{R\Lambda,R'\Lambda'}(E_1) - K_{R'\Lambda',R\Lambda}(E_2)}{E_1 - E_2}. \tag{17}$$

C. NMTO interpolation

Up to this point, we have constructed the exact (KKR) secular equation for each energy E. In the conventional LMTO approach, we can proceed to linearize the problem, i.e., to construct a variational basis by a kinked partial wave (KPW) at a certain energy E_ν and its energy derivative. Such a step leads to the relativistic version of LMTO3, which we term RLMTO3. Its formulation can be derived in a straightforward manner from the steps presented above and the nonrelativistic case discussed in Refs. 7–9. We implemented RLMTO3, and we used it for the self-consistent runs of selected applications discussed below. In the present work however, we focus on the NMTO approach. For this matter, we will discuss a different variational basis through a suitable interpolation scheme, with respect to a set of E_ν's chosen at energies $\{E_0, E_1, \ldots, E_N\}$. Once again, here we will present only the basic ideas behind NMTO; a detailed presentation can be found in Ref. 6.

Our objective is to construct, out of the energy-dependent RKPW's, a new set of energy-independent orbitals, which we call the NMTO's $\chi_{R\Lambda}$. This set of orbitals should be a good approximation to the original ones, in the sense that the pole structure of their resolvent should not deviate substantially from the ones of the KPW's. To guarantee this feature we discuss an object that acts like an orbital, but also carries information about the singularities of the resolvent. We call this object the *contracted Green's function*, and it is defined as

$$\gamma_{R\Lambda}(E,\mathbf{r}) = \sum_{R'\Lambda'} \Phi_{R'\Lambda'}(E,\mathbf{r}) G_{R'\Lambda',R\Lambda}(E), \tag{18}$$

where $G \equiv -K^{-1}$ is Green's matrix. It is easy to verify using Eq. (15), that $\gamma_{R\Lambda}(E,\mathbf{r})$ is a solution to the Dirac equation, which is smooth everywhere, except at its own (screening) sphere. At the same time, it has the same poles as Green's matrix. Moreover, any other set of orbitals $\chi(E)$ that are defined so that

$$\chi^{(N)}(E)G(E) \equiv \Phi(E)G(E) - \sum_{n=0}^{N} \Phi(E_n)G(E_n)A^{(N)}_n(E) \tag{19}$$

also have contracted Green's functions with the same poles, provided the second term is an analytical (in energy) function.

The energy-independent NMTO's are defined, if we impose the condition that

$$\chi^{(N)}(E,\mathbf{r}) = \chi^{(N)}(\mathbf{r}), \quad \forall\, E \in \{E_0, \ldots, E_N\}. \tag{20}$$

If we take the Nth order divided difference of Eq. (19) and use the condition above, we find that the NMTO's are given by

$$\chi^{(N)}(\mathbf{r}) = \frac{\Delta^N \Phi(\mathbf{r}) G}{\Delta[0\cdots N]} \left(\frac{\Delta^N G}{\Delta[0\cdots N]}\right)^{-1}, \tag{21}$$

where

$$\frac{\Delta^N f}{\Delta[0\cdots N]} \equiv f[0\cdots N] \tag{22}$$

are the divided differences of a function defined with respect to a certain mesh of discrete points. Some of the technical

details about divided differences and interpolation schemes are included in Appendix B of the present work, and in greater length, in the appendixes of Ref. 6. By expanding the divided differences of Eq. (21) we find another expression for the NMTO's,

$$\chi^{(N)}(\mathbf{r}) = \sum_{n=0}^{N} \Phi_n L_n^{(N)}, \tag{23}$$

where the matrices L_n are defined as

$$L_n^{(N)} \equiv \frac{G_n}{\prod_{m\neq n}^{N}(E_n - E_m)} G[0\cdots N]^{-1}, \tag{24}$$

and subscripts n indicate an energy E_n argument.

Here and again we see that within NMTO everything can be found through Green's matrices (which themselves are obtained from the kink matrices) and their divided differences. The same holds true for the overlap and Hamiltonian matrices (for a proof see Ref. 6), which are given as

$$\langle \chi^{(N)} | \chi^{(N)} \rangle = -G[0\cdots N]^{-1} G[[0\cdots N]] G[0\cdots N]^{-1}, \tag{25}$$

and

$$\langle \chi^{(N)} | \hat{H} - E_N | \chi^{(N)} \rangle = -G[0\cdots N]^{-1} G[[0\cdots N-1]\cdot\cdot N] \times G[0\cdots N]^{-1}, \tag{26}$$

where $G[[0\cdots M]\cdot\cdot N]$ is a Hermite divided difference (see Appendix B), and $G[[0\cdots N]] \equiv G[[0\cdots N]\cdot\cdot N]$. Because of the interpolation, the leading error of the wave function of energy ϵ_i is of order of

$$\Delta_\Psi \propto (\epsilon_i - E_0)\cdots(\epsilon_i - E_N), \tag{27}$$

and this is true for the whole space, i.e., inside WS spheres *and* in the interstitial. The single particle energies ϵ_i themselves are determined with a leading error,

$$\Delta_E \propto (\epsilon_i - E_0)^2 \cdots (\epsilon_i - E_N)^2. \tag{28}$$

It is thus obvious that by choosing the right number and positions of E_ν's we can control the error of the method and its range of validity. In the special case of a condensed mesh, the divided differences become derivatives and one can obtain again the Taylor approximation errors of LMTO, but with the order of the expansion chosen at will.

D. Spin-polarized RNMTO

In the spin-polarized case, as discussed in Appendix A, a partial wave φ_R has, away from the nucleus, two components κ_1 and κ_2. Such a function carries indexes λ and μ, with the μ indexes omitted here for clarity. This partial wave is integrated outward until the s_R radius. Then we integrate the free Dirac equation inward to find φ_R^0, which now, likewise, has two κ components. The inward integration is similar to the nonspin polarized case, with the initial condition that it matches for the value of the upper and lower parts to *each* κ *component* of φ. In other words, the values of the radial parts of φ provide the initial boundary conditions for the inward integration in free space. Since the free Dirac equation does not contain a magnetic-field term, the two κ differential equations decouple, and they are performed independently. However, unlike as in the nonspin-polarized case, we are faced with the question of how to match the $\varphi_{R,\lambda}^0$ solutions, which, as we mentioned above, have a mixed κ character, to the interstitial solutions $\Psi_{R,\kappa}$ of single κ at the a sphere. For this to become possible, we define new solutions $\phi_{R,\kappa}^0$,

$$\phi_{R,\kappa}^0 = \sum_{\lambda=\lambda_1,\lambda_2} N_{R,\kappa\lambda} \varphi_{R,\lambda}^0, \tag{29}$$

with the matrix N chosen so that

$$\phi_{1,\kappa\kappa'}^0(a_R) = \delta_{\kappa,\kappa'}. \tag{30}$$

The matrix N is then given by

$$N_{R,\kappa\lambda} = G_{R,\lambda\kappa}^{-1}, \quad G_{R,\lambda\kappa} = \begin{bmatrix} \varphi_{1,\lambda_1\kappa_1}^0(a_R) & \varphi_{1,\lambda_1\kappa_2}^0(a_R) \\ \varphi_{1,\lambda_2\kappa_1}^0(a_R) & \varphi_{1,\lambda_2\kappa_2}^0(a_R) \end{bmatrix}. \tag{31}$$

In the above, $\phi_{1,\kappa\kappa'}^0$ and $\varphi_{1,\lambda\kappa'}^0$ denote the κ' component of the upper part of the ϕ_κ^0 and φ_λ^0, respectively. With this generalized normalization, the upper components of ϕ_κ^0 can be matched (κ) channel-by-channel to a Ψ_κ, as far as the value is concerned. However, there are still kinks in both κ channels that have to be canceled. The kink that φ_κ^0 has in the κ' channel is given by

$$D_{R,\kappa\kappa'} - S_{R\kappa,R\kappa'}, \tag{32}$$

where

$$D_{R,\kappa\kappa'} = \sum_{\lambda} N_{R,\kappa\lambda} G'_{R,\lambda\kappa'}. \tag{33}$$

In the above G' is the matrix of radial derivatives corresponding to G. The main difference with respect to the nonspin-polarized case is the fact that the previously diagonal, logarithmic, derivative contribution to the kink matrix has itself become a matrix. Otherwise the situation is completely equivalent, and this means that once we construct the appropriate kink matrices corresponding to Eq. (32), we can apply the same interpolation NMTO scheme, through the introduction of contracted Green's functions and their divided differences.

III. APPLICATIONS

In this section we present the results for selected applications of the formalism discussed above. First, we study the nonmagnetic semiconductors GaAs and InSb. Second, and as a test of the spin-polarized case, we present the band structure of bcc Fe and δ-Pu. Since the purpose of the present work is to demonstrate the accuracy and applicability of the new, relativistic NMTO method, we focus on numerical

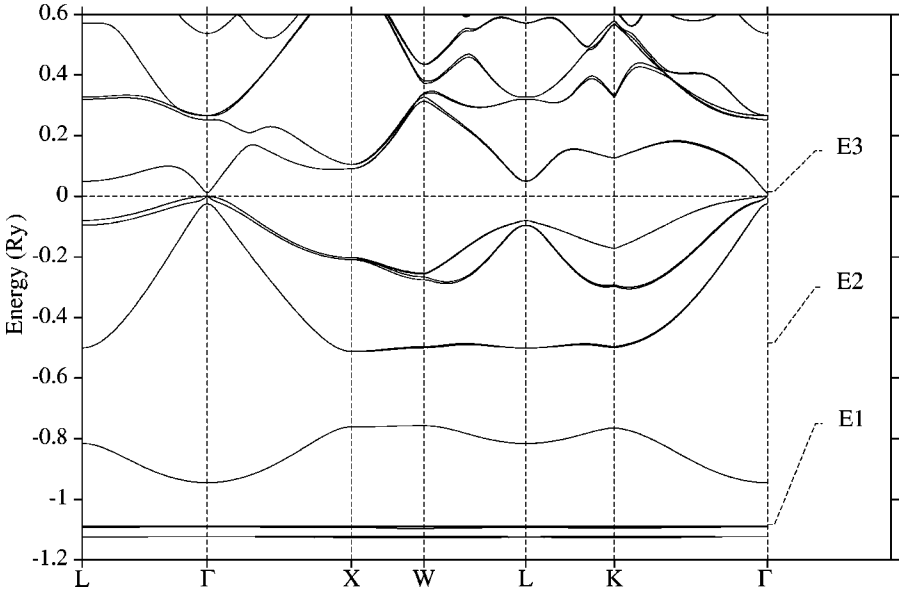

FIG. 1. RNMTO band structure of GaAs. The number and positions of E_ν's are shown on the right of the figure. Zero is chosen at the Fermi level.

comparisons of our RNMTO results with the results from other relativistic approaches. In all cases we use the local-denisity approximation (LDA) functional of Hedin and Lundqvist,[20] without any relativistic corrections for the description of exchange and correlation. To fulfill the space-filling requirement, empty spheres are introduced whenever necessary.

A. Non-spin-polarized

We start our applications with the broadband semiconductor GaAs. Even for the relatively light elements Ga and As, relativistic effects, e.g., spin-orbit splittings, are not negligible. The RNMTO band structure of GaAs in its equilibrium, zinc-blende phase is given in Fig. 1. We use the experimental lattice constant of 5.654 Å and a potential generated by RLMTO3 with Ga 4*s*4*p*3*d*, As 4*s*4*p*4*d* as valence states. For the band calculations with RNMTO, As-*f* states are also included in the orbital set. For the empty spheres we include *spd* orbitals, with the *p* and *d* treated as intermediate and downfolded. In generating the potential one generally makes a choice of which levels to treat as core states, and this is the meaning of the main quantum numbers appearing in the description of valence states. It must be stressed, however, that the main quantum numbers are not an input to the NMTO-band calculation; rather, the corresponding continuous number P_ν is determined for a given potential by the selection of E_ν's. One of the strengths of NMTO is that it can treat with a single diagonalization hybridization effects that correspond to successive atomic levels. In the case of GaAs, our secular matrix can describe hybridization with the semicore Ga 3*d* states, as well as with high-lying Ga 4*d* states.

In Table I we present a quantitative comparison between different calculations that demonstrate the applicability of RNMTO. The comparison is performed for a selection of high-symmetry points and their corresponding levels, the symbols of which are given in column 1. In column 2 we present the results of a relativistic-panel-LMTO-ASA calculation obtained by Bachelet and Christensen[21] using the LDA functional of Ceperley and Adler as parametrized by Perdew and Zunger. Column 3 has the results of a relativistic full potential KKR method (RFKKR) by BeiderKellen and Freeman,[22] using the LDA functional of Hedin-Lundqvist. In column 4 (5) we present the results obtained with RNMTO and with 2 (3) E_ν's chosen at −14.75 eV, −1.14 eV (−14.75 eV, −6.58 eV, 0.22 eV), respectively. The zero of the energy scale is chosen at the valence-band maximum (VBM) found at Γ_{15v}.

We have chosen to compare our results to those of panel LMTO and KKR, since these methods obtain band energies with minimal errors throughout the band spectrum. As one can deduce from the results in Table I, RNMTO can provide energies with a similar level of accuracy and still retain a small basis set. The small discrepancies with respect to RFKKR, more pronounced for higher orders of representation, can be explained because of the use of spherical potentials within the WS spheres. One particular feature to be mentioned is the value of the gap (0.12 eV), which is in excellent agreement with the result of RFKKR. Of course this value is not close the experimental one ($\approx$1.42 eV), but this discrepancy is based on a well-known deficiency of the local density approximation. It should be pointed out that this value for the gap can be found only if the Ga 3*d* semicore states are included as valence states both in the creation of the potential and also in a single secular matrix. If one generates the potential with Ga 3*d* treated as core states, or if one uses different panels for the 3*d* energy range and the VBM range, then the calculated gap is 0.25 eV. The latter scenario explains the discrepancy of the gap between column 2 and the other columns,[23]

It is also notable that RNMTO is in good agreement with RFKKR, even for high unoccupied states, such as Γ_{15c}, X_{1c}, X_{3c}, and especially L_{3c}. From inspection of the bands in Fig. 1, we conclude that this agreement persists for states at least up to $\approx$7 eV above the Fermi level and for all high-symmetry lines. As a matter of fact, the range and degree of agreement can be adjusted at will by choosing the appropri-

TABLE I. Energy levels of GaAs (in eV) at Γ, X, and L.

Level	RLMTO[a]	RFKKR[b]	RNMTO[c]	RNMTO[d]
Γ_{1v}	−12.85	−12.94	−12.87	−12.87
Γ_{15v}	−0.36	−0.35	−0.35	−0.35
	0.00	0.00	0.00	0.00
Γ_{1c}	0.25	0.12	0.13	0.14
Γ_{15c}		3.46	3.48	3.43
		3.66	3.69	3.63
X_{1v}	−10.49	−10.42	−10.35	−10.37
X_{3v}	−7.06	−7.02	−6.96	−6.98
X_{5v}	−2.90	−2.88	−2.83	−2.84
	−2.83	−2.79	−2.75	−2.75
X_{1c}	1.05	1.17	1.24	1.24
X_{3c}	1.28	1.39	1.44	1.43
L_{1v}	−11.20	−11.18	−11.09	−11.11
L_{1v}	−6.94	−6.83	−6.81	−6.82
L_{3v}	−1.39	−1.38	−1.31	−1.30
	−1.18	−1.17	−1.10	−1.09
L_{1c}	0.67	0.71	0.66	0.66
L_{3c}		4.38	4.56	4.36
		4.46	4.67	4.45

[a]Panel LMTO, Ref. 21.
[b]Relativistic full potential KKR, Ref. 22.
[c]RNMTO, 2 E_v's at −14.75 eV and −1.14 eV.
[d]RNMTO, 3 E_v's at −14.75 eV, −6.58 eV, and 0.22 eV.

ate number and positions for E_ν's. We see by comparing the last two columns that the inclusion of one extra E_ν at an unoccupied level has brought the results of column 5 in significantly closer agreement to KKR, with respect to those of column 4.

As a second application of our RNMTO, we have chosen InSb. The band structure of InSb in its equilibrium, zinc-blende phase is given in Fig. 2. We have used the experimental lattice constant of 6.478 Å and the potential generated self-consistently using RLMTO3 with In

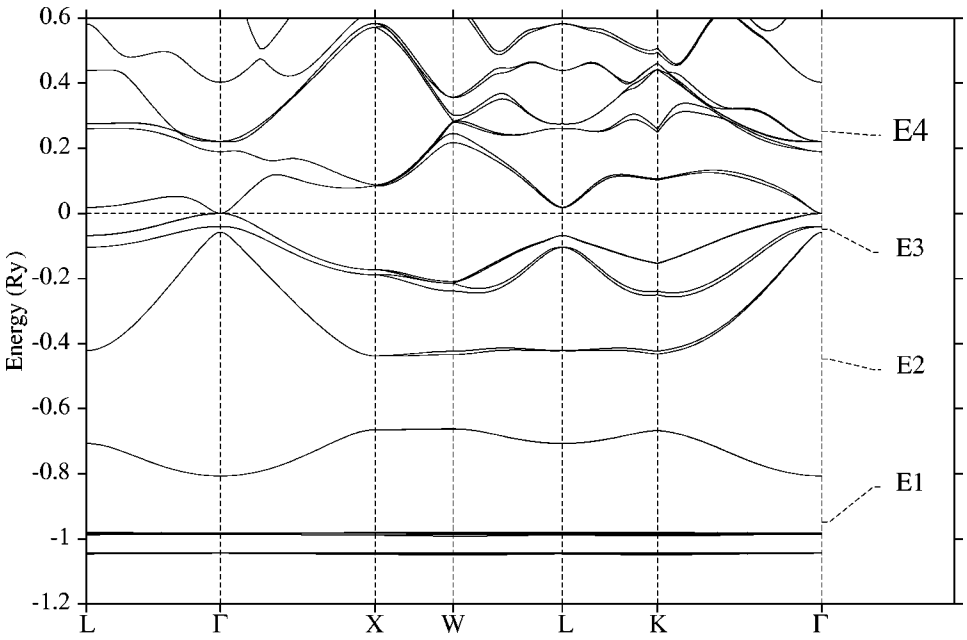

FIG. 2. RNMTO band structure of InSb. The number and positions of E_ν's are shown on the right of the figure. Zero is chosen at the Fermi level.

TABLE II. Energy levels of InSb (in eV) at Γ, X, and L.

Level	RFKKR[a]	RNMTO[b]	RNMTO[c]
Γ_{25v}	−15.15	−15.21	−15.24
	−14.34	−14.41	−14.42
Γ_{12v}	−14.26	−14.38	−14.38
Γ_{1v}	−11.05	−10.97	−10.97
Γ_{15v}	−0.77	−0.77	−0.77
	0.00	0.00	0.00
Γ_{1c}	−0.66	−0.74	−0.74
Γ_{15c}	2.39	2.48	2.38
	2.83	2.97	2.83
X_{1v}	−9.05	−8.97	−8.97
X_{3v}	−6.24	−6.15	−6.17
X_{5v}	−2.67	−2.59	−2.59
	−2.49	−2.41	−2.41
X_{1c}	0.91	1.06	1.04
X_{3c}	0.94	1.07	1.04
L_{1v}	−9.68	−9.57	−9.59
L_{1v}	−5.93	−5.88	−5.89
L_{3v}	−1.53	−1.44	−1.44
	−1.05	−0.95	−0.95
L_{1c}	0.15	0.09	0.09
L_{3c}	3.33	3.91	3.40
	3.51	4.22	3.59

[a]Relativistic full potential KKR, Ref. 22.
[b]RNMTO, 2 E_v's at −13.32 eV and −1.07 eV.
[c]RNMTO, 4 E_v's at −13.32 eV, −6.52 eV, −1.07 eV, and 3.01 eV.

5*s*5*p*4*d*4*f* (4*f* downfolded), Sb 5*s*5*p*5*d*4*f* (5*d*4*f* downfolded), and *spd* for the empty spheres (*pd* downfolded). The same set of orbitals was chosen for the band calculations using RNMTO.

The results from our own calculations for certain levels are again compared with those of RFKKR[22] in Table II. Column 2 has the results of RFKKR, and column 3 (4) the RNMTO results with 2 (4) E_v's at −13.32 eV and −1.07 eV (−13.32 eV, −6.52 eV, −1.07 eV, and 3.01 eV). This comparison reinforces the validation of our approach. Especially when the spectrum is considered as a whole, the advantage of RNMTO becomes apparent in providing even the high unoccupied states such as Γ_{15c} and L_{3c}. We should once again point out that the poor value of the gap obtained (for InSb it is even negative, −0.74 eV) in these calculations can be traced to the deficiencies of LDA, and just as for GaAs, no effort to correct it was undertaken.

B. Spin-polarized

The first test case for our spin-polarized RNMTO (SRNMTO) is ferromagnetic, bcc Fe. The lattice constant used is 2.861 Å and the valence-state orbital set consists of *spd* orbitals. The spin-polarized potential was obtained with a scalar-relativistic tight-binding (TB) LMTO-ASA code, which gave a magnetic moment of $2.23\mu_B$. With this potential we have calculated the band structure with the magnetization along the [001] direction. A detail of the band structure around the Γ point, and close to the Fermi level, is given in Fig. 3. Since Fe is not a particularly heavy metal, its band structure is almost the same as a superposition of the majority and minority bands from a standard nonrelativistic calculation. The inclusion of spin-orbit effects alters the nonrelativistic bands only slightly by providing extra anticrossing features, as shown in Fig. 3. This picture compares very well with the one obtained by Lovatt *et al.*[24] using a non-self-consistent, full-potential KKR method. We see that in the presence of a magnetic field, all degeneracies, including time reversal, are lifted at the high-symmetry points. (There is indeed a very small splitting for point P.) Even though the apparent splittings are very small, they play a defining role for interesting properties such as magnetocrystalline anisotropy, magnetic dichroism, and the optical Kerr effect. In particular, for the latter optical properties, SRNMTO can provide a useful tool to obtain the spectra, even for states that lie high above the Fermi level.

As a second test for SRNMTO, we have used the case of δ-Pu. The δ phase of Pu corresponds to an fcc structure, and it is one of the Pu phases found at high temperatures. In Fig.

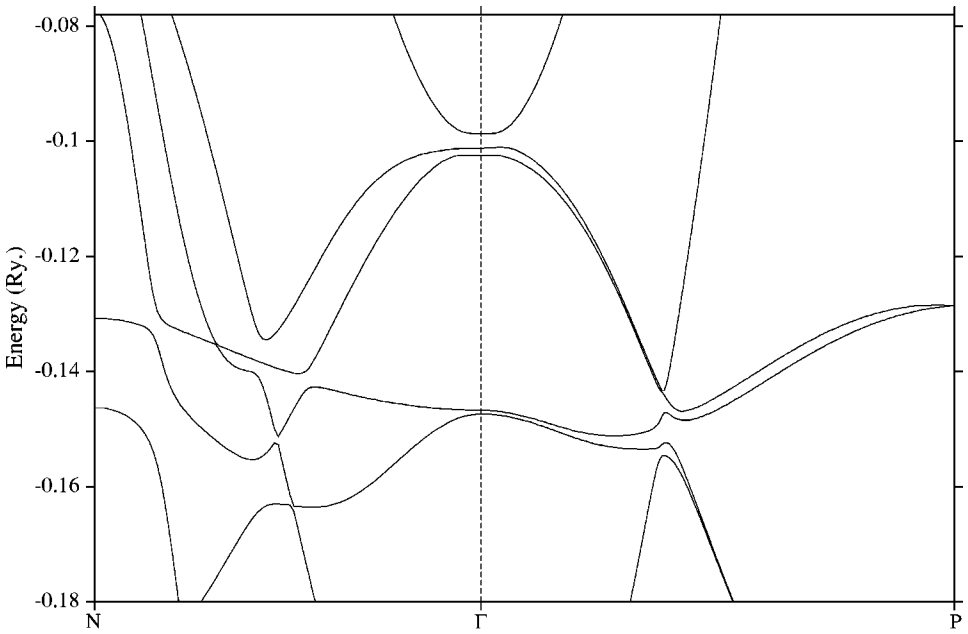

FIG. 3. Detail of the SRNMTO band structure of ferromagnetic bcc Fe with magnetization along the [001] axis. Zero is chosen at the Fermi level.

4 we give a detail of the band structure calculated at a lattice constant of 4.63 Å with *spdf* orbitals included. The spin-polarized potential was again taken from a nonrelativistic calculation using TB-LMTO-ASA and the magnetization points along the [001] axis. In generating the potential the spin-orbit coupling was included self-consistently at the variational step. The detail given here is in excellent agreement with the bands obtained by Solovyev *et al.*,[17] using a self-consistent, spin-polarized, relativistic version of LMTO-ASA. In particular the figure shows the big magnetocrystalline anisotropy along the ΓX and ΓZ directions. These directions would be otherwise equivalent in the nonrelativistic or the nonmagnetic case.

The physical properties of different phases of Pu have attracted considerable attention in the last few years. As we mentioned before, it is not the aim of the present paper to dwell on such interesting properties related to correlated phenomena (see for example Ref. 25 and references therein). Also, a highly accurate description of Pu and similar structures entails self-consistent calculations based on a full-potential scheme and inclusion of orbital polarization and spin disorder.[26] The development of such a scheme, however, lies outside the scope of the present work, which has as a well-defined task: the discussion of the relativistic version of the third generation LMTO and NMTO methods. In this respect, we have used δ-Pu as a typical example of a narrow-band system, where a set of E_ν's can be chosen to obtain the bands ranging from the low-lying 6*p* states to states high above the Fermi level. It must be pointed out that the proper switching behavior in NMTO

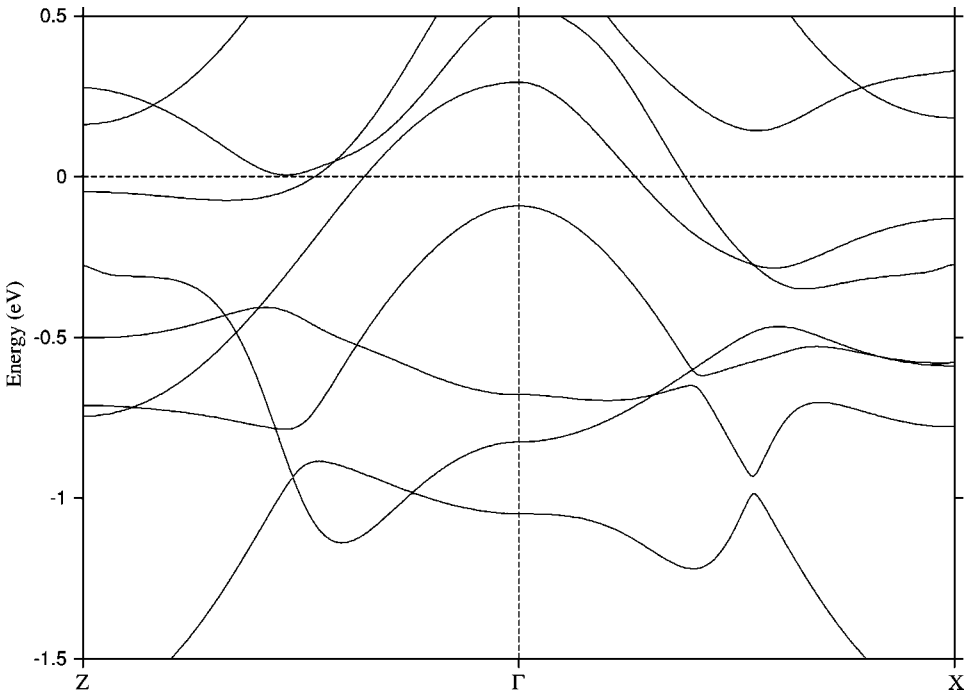

FIG. 4. SRNMTO band structure of ferromagnetic δ-Pu with magnetization along the [001] axis (in units of $2\pi/a$). E_ν's at −26.25 eV, −20.12 eV, −4.49 eV, and 4.35 eV. Zero is chosen at the Fermi level.

from one level to the other depends on the selection of E_ν's. They must be positioned within a reasonable range of the band (or bands) to be described. It is therefore clear that more caution is to be exercised in the case of a narrow-band system, in order to avoid wrong switching behavior between different levels. Similarly, caution is needed also in the selection of the augmentation (screening sphere) radii.[6] In case of switching problems, the procedure of downfolding, which has been used in previous approaches of LMTO and has been adopted easily in RNMTO as well, can provide a solution.

IV. SUMMARY

In the present paper we discussed the fully relativistic version of the NMTO method. The formalism is a rather straightforward generalization of the nonrelativistic one discussed recently by Andersen and co-workers. At the same time, the current paper provides the necessary steps for a relativistic version for the earlier-developed third generation LMTO. All the important quantities can be expressed using the relativistic kink matrices, through which the matching conditions on the screening spheres is defined. The applicability of the method has been demonstrated through a series of examples. First, we used as test cases two broadband semiconductors, GaAs and InSb. For the spin-polarized case, we obtained the band structures of bcc Fe and δ-Pu. The advantage of NMTO in describing the bands accurately in a broad-energy range is clearly established.

ACKNOWLEDGMENTS

We thank Professor Ole Krogh Andersen for comments on the manuscript and for useful discussions. We also thank members of the Stuttgart group, especially Dr. Sergei Ezhov and Dr. Dmitri Savrasov, for fruitful discussions on the NMTO method and its implementation.

APPENDIX A: DIRAC EQUATION SOLUTIONS

1. No magnetic field

The Dirac Equation has the form

$$\hat{H}_0\Psi = E_i\Psi, \tag{A1}$$

where

$$\hat{H}_0 = c\alpha\cdot\mathbf{p} + (\beta - I_4)mc^2 + V(\mathbf{r})I_4, \tag{A2}$$

and

$$\alpha = \begin{pmatrix} 0 & \sigma \\ \sigma & 0 \end{pmatrix}, \quad \beta = \begin{pmatrix} I_2 & 0 \\ 0 & -I_2 \end{pmatrix}, \tag{A3}$$

with σ being the vector of the Pauli matrices. In a central field, the Dirac Hamiltonian $\hat{H}_0$ commutes with the following operators:

$$[H_0, J^2] = 0, \quad [H_0, J_z] = 0, \quad [H_0, S^2] = 0, \quad [H_0, K] = 0, \tag{A4}$$

where $J(S)$ is the total (spin) angular momentum, and $K = \beta(\sigma\cdot\mathbf{L} + 1)$.

Based on the commutation relations of Eq. (A4), the solution of the Dirac Equation in a central field has the form of

$$\Phi_\Lambda(E,\mathbf{r}) = \begin{bmatrix} g_\kappa(E,r)\Omega_{\kappa\mu}(\hat{\mathbf{r}}) \\ if_\kappa(E,r)\Omega_{-\kappa\mu}(\hat{\mathbf{r}}) \end{bmatrix}, \quad \Lambda = (\kappa,\mu). \tag{A5}$$

In the above, the κ's assume the following values:

$$\kappa = \begin{cases} -l-1 & \text{for} \quad j = l + 1/2 \\ l & \text{for} \quad j = l - 1/2 \end{cases}, \quad \kappa = \pm 1, \pm 2, \pm 3, \ldots, \tag{A6}$$

and j,μ are the quantum numbers of $\mathbf{J}$ and its z projection, respectively.

The spin-spherical harmonics $\Omega_{\kappa\mu}$ are defined as

$$\Omega_{\kappa\mu}(\hat{\mathbf{r}}) = \sum_{\sigma=\pm 1/2} c\left(lj\frac{1}{2}; \mu-\sigma, \sigma\right) Y_{l,\mu-\sigma}(\hat{\mathbf{r}})\varphi_\sigma, \tag{A7}$$

where φ_σ are the spin functions, $Y_{l,m}$ are the spherical harmonics, and $c\left(lj\frac{1}{2}; \mu-\sigma, \sigma\right)$ are the Clebsch-Gordan coefficients for spin $\frac{1}{2}$.

The radial parts $g_\kappa(E,r)$, $f_\kappa(E,r)$ satisfy a set of differential equations,

$$\frac{dg_\kappa}{dr} = -\frac{1+\kappa}{r}g_\kappa - \left[1 + \frac{E - V(r)}{c^2}\right]cf_\kappa, \tag{A8}$$

$$c\frac{df_\kappa}{dr} = -\frac{1-\kappa}{r}cf_\kappa + [E - V(r)]g_\kappa, \tag{A9}$$

and certain initial conditions,

$$\begin{pmatrix} g_\kappa(E,r) \\ f_\kappa(E,r) \end{pmatrix} \propto Ar^\alpha \begin{pmatrix} 1 \\ q \end{pmatrix}, \tag{A10}$$

where

$$\alpha = -1 + [\kappa^2 - (2Z/c)^2]^{1/2}, \quad q = \frac{c}{2Z}(\kappa + 1 + \alpha). \tag{A11}$$

If we have an empty sphere ($Z=0$), then the initial condition is

$$\begin{pmatrix} g_\kappa(E,r) \\ f_\kappa(E,r) \end{pmatrix} \propto A\begin{pmatrix} r^l \\ \dfrac{\kappa+1+l}{c\gamma}r^{l-1} \end{pmatrix}, \quad \gamma = 1 + \frac{E - V(0)}{c^2} \tag{A12}$$

2. With magnetic field

In the presence of a magnetic field (external+internal), only μ remains a good quantum number and the solutions to the Dirac Equation are given by

$$\Phi_{\lambda\mu}(E) = \sum_{\kappa=\kappa_1,\kappa_2} \begin{pmatrix} g_{\kappa\lambda\mu}(E)\Omega_{\kappa\mu} \\ if_{\kappa\lambda\mu}(E)\Omega_{-\kappa\mu} \end{pmatrix}. \tag{A13}$$

The radial parts $g_\kappa(E,r)$, $f_\kappa(E,r)$ satisfy a set of differential equations,

$$\left(\frac{d}{dr} + \frac{1+\kappa}{r}\right) g_\kappa - \left[1 + \frac{E - V(r)}{c^2}\right] c f_\kappa = \frac{B(r)}{c^2} \sum_{\kappa'} \langle -\kappa\mu|\sigma_z|-\kappa'\mu\rangle c f_{\kappa'}, \tag{A14}$$

$$\left(\frac{d}{dr} + \frac{1-\kappa}{r}\right) c f_\kappa - [E - V(r)] g_\kappa = B(r) \sum_{\kappa'} \langle \kappa\mu|\sigma_z|\kappa'\mu\rangle g_{\kappa'}. \tag{A15}$$

In general, the last terms in the above set of equations couple any κ solutions to any other κ'. However, using a standard approximation, we retain only terms that couple the two κ's (say κ_1,κ_2) and that correspond to the same l. Then a way of defining linearly independent λ solutions is to apply the initial condition that a λ_1 (λ_2) solution has only a κ_1 (κ_2) component close to the nucleus.

3. Relation of kinks to discontinuities

Let $S^\alpha_{R'\Lambda',R\Lambda}$ denote the value (times the velocity of light c) of the lower component of $N^\alpha_{R\Lambda}$ on the $a_{R\Lambda}$ sphere. Let also $T^\alpha_{R'\Lambda',R\Lambda}$ denote the slope of the upper component of $N^\alpha_{R\Lambda}$ on the $a_{R\Lambda}$ sphere. For the free $[V(r)=0]$ Dirac equation we have

$$c f(a_{R\Lambda}) = \frac{1}{\gamma}\left[g'(a_{R\Lambda}) + \frac{1+\kappa}{a_{R\Lambda}} g(a_{R\Lambda})\right], \tag{A16}$$

and therefore,

$$S^\alpha_{R'\Lambda',R\Lambda} = \frac{1}{\gamma}\left[J^{\alpha'}_{1,R'\Lambda'}(a_{R'\Lambda'}) + \frac{1+\kappa}{a_{R'\Lambda'}} \overbrace{J^\alpha_{1,R'\Lambda'}(a_{R'\Lambda'})}^{0}\right] T^\alpha_{R'\Lambda',R\Lambda} + \frac{1}{\gamma}\left[N^{\alpha'}_{1,R\Lambda}(a_{R\Lambda}) + \frac{1+\kappa}{a_{R\Lambda}} \overbrace{N^\alpha_{1,R\Lambda}(a_{R\Lambda})}^{1}\right] \delta_{R\Lambda,R'\Lambda'}. \tag{A17}$$

If we impose the conditions $N^{\alpha'}_{1,R\Lambda}(a_{R\Lambda})=0$ and $J^{\alpha'}_{1,R\Lambda}(a_{R\Lambda})=1$, then the matrix $S^\alpha_{R'\Lambda',R\Lambda}$ will give at the same time both the slope of the upper component and the value of the lower component of the Λ' projection of a relativistic SSW $\Psi_{R\Lambda}$ on the $\alpha_{R'\Lambda'}$ sphere, with only a diagonal-term difference between the two and a scaling factor $\gamma \approx 1$. The diagonal term can be combined with the value of the lower component of the partial wave φ to lead to the so-called relativistic logarithmic derivative,[12–15,19]

$$D_\kappa(E) = sc\frac{f_\kappa(E,s)}{g_\kappa(E,s)} - \kappa - 1. \tag{A18}$$

It is thus clear that the secular Eq. (14) eliminates both the kinks of the upper components and the discontinuities of the lower components.

APPENDIX B: INTERPOLATION THROUGH DIVIDED DIFFERENCES

Given a function $f(\epsilon)$ and a discrete set of points $\{\epsilon_m, \epsilon_{m+1}, \ldots, \epsilon_n, \epsilon_{n+1}, \ldots, \epsilon_N\}$, the divided differences of f are defined by the following:

$$f[m, m+1, \ldots, n+1] \equiv \frac{f[m, \ldots, n] - f[m+1, \ldots, n+1]}{\epsilon_m - \epsilon_{n+1}}, \tag{B1}$$

where $m \leqslant n$ and $f[m,m] \equiv f(\epsilon_m)$. The approximating polynomial of order N that has the same values as function $f(\epsilon)$ on a set of points $\{\epsilon_0, \epsilon_1, \ldots, \epsilon_N\}$ is given by

$$f^{(N)}(\epsilon) = \sum_{M=0}^{N} f[0 \cdots M] \prod_{n=0}^{M-1} (\epsilon - \epsilon_n). \tag{B2}$$

If we expand the right side of Eq. (B1) we obtain the important relation (Lagrange form of the divided differences),

$$f[0 \cdots M] = \sum_{n=0}^{M} \frac{f_n}{\prod_{m=0,\neq n}^{M} (\epsilon_n - \epsilon_m)}. \tag{B3}$$

For the product of the two functions $f(\epsilon)$ and $g(\epsilon)$ defined on the same mesh of points, we obtain, by using Eq. (B3), the binomial formula,

$$(fg)[0 \cdots N] = \sum_{M=0}^{N} f[0 \cdots M] g[M \cdots N]. \tag{B4}$$

It is easy to show that for a mesh that condenses around a certain point ϵ_ν, the Newton interpolation is equivalent to a Taylor expansion of the same order.

Another interpolating scheme is the so-called *Hermite interpolation*. In this case, the approximating polynomial matches not only the values of a function f at certain points $\{\epsilon_i\}$, but also the derivatives of f. Given the values at a set $\{\epsilon_0, \ldots \epsilon_N\}$ and the slopes at its subset $\{\epsilon_0, \ldots \epsilon_M\}$ the Hermite interpolating polynomial is given by

$$f^{(N+M+1)}(\epsilon) = \sum_{n=0}^{M} \left\{ f_n + \left[\dot{f}_n - f_n \left(\sum_{m=0,\neq n}^{M} \frac{2}{\epsilon_n - \epsilon_m} + \sum_{m=M+1}^{N} \frac{1}{\epsilon_n - \epsilon_m} \right) \right] (\epsilon_n - \epsilon_m) \right\} l_n^{(M)}(\epsilon) l_n^N(\epsilon) + \sum_{n=M+1}^{N} f_n l_n^{(M+1)}(\epsilon) l_n^N(\epsilon), \tag{B5}$$

where

$$l_n^N(\epsilon) \equiv \prod_{m=0,\neq n}^{N} \frac{\epsilon - \epsilon_m}{\epsilon_n - \epsilon_m}. \tag{B6}$$

The coefficient corresponding from $f^{(N+M+1)}(\epsilon)$ to the highest power of ϵ defines the *Hermite divided differences*, which can be expressed through the Newton divided differences as

$$f[(0\cdots M]\cdot\cdot N) = \sum_{n=0}^{N}\sum_{n'=0}^{M} \frac{f[n,n']}{\prod_{m=0,\neq n}^{N}(\epsilon_n - \epsilon_m)\prod_{m'=0,\neq n'}^{M}(\epsilon_{n'} - \epsilon_{m'})}. \tag{B7}$$

In Eq. (B7) the special case $n \to n'$ means that the corresponding divided difference becomes the derivative.

*Present address: Department of Physics and Astronomy, Vanderbilt University, Nashville, TN 37235.

[1] O. K. Andersen, Phys. Rev. B **12**, 3060 (1975).

[2] O. K. Andersen and O. Jepsen, Phys. Rev. Lett. **53**, 2571 (1984).

[3] O. K. Andersen, O. Jepsen, and D. Glötzel, in *Highlights of Condensed Matter Theory*, edited by F. Bassani, F. Fumi, and M. P. Tosi (North-Holland, New York, 1985); O. K. Andersen, O. Jepsen, and M. Sob, in *Lecture Notes in Physics: Electronic Band Structure and Its Applications*, edited by M. Yussouf (Springer-Verlag, Berlin, 1987).

[4] M. Methfessel, Phys. Rev. B **38**, 1537 (1988); M. Methfessel, C. O. Rodriguez, and O. K. Andersen, *ibid.* **40**, 2009 (1989).

[5] S. Y. Savrasov, Phys. Rev. B **54**, 16470 (1996).

[6] O. K. Andersen, T. Saha-Dasgupta, R. W. Tank, C. Arcangeli, O. Jepsen, and G. Krier, in *Electronic Structure and Physical Properties of Solids. The Uses of the LMTO Method*, edited by H. Dreyssé (Springer, Berlin, 2000), 3–84.

[7] O. K. Andersen, C. Arcangeli, R. W. Tank, T. Saha-Dasgupta, G. Krier, O. Jepsen, and I. Dasgupta, in *Tight Binding Approach to Computational Materials Science*, edited by L. Colombo, A. Gonis, and P. Turchi, MRS Symposia Proceedings Series No. 491, Materials Research Society, Pittsburgh, 1998, pp. 3–34.

[8] R. Tank and C. Arcangeli, Phys. Status Solidi B **217**, 89 (2000).

[9] L. Vitos, H. L. Skriver, B. Johansson, and J. Kollar, Comput. Mater. Sci. **18**, 24 (2000); L. Vitos, Phys. Rev. B **64**, 014107 (2001).

[10] O. K. Andersen and T. Saha-Dasgupta, Phys. Rev. B **62**, R16219 (2000); O. K. Andersen, T. Saha-Dasgupta, and S. Ezhov, Bull. Mater. Sci. **26**, 19 (2003).

[11] E. Pavarini, S. Biermann, A. Poteryaev, A. L. Lichtenstein, A. Georges, and O. K. Andersen, Phys. Rev. Lett. **92**, 176403 (2004).

[12] C. Godreche, J. Magn. Magn. Mater. **29**, 262 (1982).

[13] V. V. Nemoshkalenko, A. E. Krasovski, V. N. Antonov, Vl. N. Antonov, U. Fleck, H. Wonn, and P. Ziesche, Phys. Status Solidi B **120**, 283 (1983).

[14] N. E. Christensen, Int. J. Quantum Chem. **25**, 255 (1984).

[15] H. Ebert, Phys. Rev. B **38**, 9390 (1988).

[16] M. Pénicaud, in *Shock Waves in Condensed Matter*, edited by J. R. Asay, R. A. Graham, and G. K. Straub (Elsevier, Amsterdam, 1984).

[17] I. V. Solovyev, A. I. Liechtenstein, V. A. Gubanov, V. P. Antropov, and O. K. Andersen, Phys. Rev. B **43**, 14 414 (1991).

[18] M. E. Rose, *Relativistic Electron Theory* (Wiley, New York, 1961).

[19] I. Turek, V. Drchal, J. Kudrnovsky, M. Sob, P. Weinberger, *Electronic Structure of Disordered Alloys, Surfaces, and Interfaces* (Kluwer Academic Publishers, Dordrecht, 1997).

[20] L. Hedin and B. I. Lundqvist, J. Phys. C **4**, 2064 (1971).

[21] G. B. Bachelet and N. E. Christensen, Phys. Rev. B **31**, 879 (1985).

[22] S. BeiderKellen and A. J. Freeman, Phys. Rev. B **54**, 11187 (1996).

[23] N. E. Christensen (private communication).

[24] S. C. Lovatt, B. L. Gyoffry, and G.-Y. Guo, J. Phys.: Condens. Matter **5**, 8005 (1993).

[25] S. Y. Savrasov and G. Kotliar, Phys. Rev. Lett. **84**, 3670 (2000); S. Y. Savrasov, G. Kotliar, E. Abrahams, Nature (London) **410**, 793 (2001).

[26] P. Söderlind, A. L. Landa, and B. Sadigh, Phys. Rev. B **66**, 205109 (2002); A. Landa and P. Söderlind, Condens. Matter Phys. **7**, 247 (2004).